Revision 2

Alumino-oxy-rossmanite from pegmatites in Variscan metamorphic rocks from Eibenstein an der Thaya, Lower Austria, Austria: a new tourmaline that represents the most Al-rich end-member composition

ANDREAS ERTL[1ξ], JOHN M. HUGHES[2], STEFAN PROWATKE[3,4], THOMAS LUDWIG[4], CHRISTIAN L. LENGAUER[1], HANS-PETER MEYER[4], GERALD GIESTER[1], UWE KOLITSCH[5,1], AND ALBERT PRAYER[6]

[1] Institut für Mineralogie und Kristallographie, Geozentrum, Universität Wien, Althanstrasse 14, 1090 Wien, Austria

[2] Department of Geology, University of Vermont, Burlington, VT 05405, U.S.A.

[3] D. Swarovski KG, Swarovskistrasse 30, 6112 Wattens, Austria

[4] Institut für Geowissenschaften, Universität Heidelberg, Im Neuenheimer Feld 234–236, 69120 Heidelberg, Germany

[5] Mineralogisch-Petrographische Abt., Naturhistorisches Museum, Burgring 7, 1010 Vienna, Austria

[6] Sportplatzgasse 8, 3754 Irnfritz, Austria

[ξ] *corresponding author*: andreas.ertl@a1.net

ABSTRACT

Alumino-oxy-rossmanite, ideally □$Al_3Al_6(Si_5AlO_{18})(BO_3)_3(OH)_3O$, is here described as a new member of the tourmaline supergroup. It is an early-magmatic Al-rich oxy-tourmaline from a small pegmatitic body embedded in amphibolite and biotite-rich paragneiss. This new pink tourmaline was found in a Moldanubian pegmatite (of the Drosendorf Unit) that occurs in a large quarry near the village of Eibenstein an der Thaya, Waidhofen an der Thaya district, Lower Austria, Austria. The empirical formula of the holotype was determined on the basis of electron-microprobe analysis (EMPA), secondary-ion mass spectrometry (SIMS), spectroscopical methods (optical absorption and infrared spectroscopy), and crystal-structure refinement (SREF) as $^{X}(□_{0.53}Na_{0.46}Ca_{0.01})$ $^{Y}(Al_{2.37}Mn^{3+}_{0.21}Li_{0.16}□_{0.14}Mn^{2+}_{0.07}Fe^{3+}_{0.03}Fe^{2+}_{0.01}Ti^{4+}_{0.01})$ $^{Z}Al_6$ $(Si_{5.37}Al_{0.41}B_{0.22}O_{18})(BO_3)_3$ $^{V}[(OH)_{2.77}O_{0.23}]$ $^{W}[O_{0.80}(OH)_{0.15}F_{0.05}]$. Chemical composition (wt%) is: SiO_2 33.96, TiO_2 0.10, Al_2O_3 47.08, B_2O_3 11.77, FeO 0.08, Fe_2O_3 0.23, MnO 0.52, Mn_2O_3 1.70, CaO 0.04, Li_2O 0.25, ZnO 0.03, Na_2O 1.51, H_2O 2.79, F 0.09, total 100.11. The presence of relatively high amounts of trivalent Mn in alumino-oxy-rossmanite is in agreement with the observation that the OH groups are present at a lower concentration than commonly found in other Al-rich and Li-bearing tourmalines. The crystal structure of alumino-oxy-rossmanite (space group *R*3*m*; *a* = 15.803(1), *c* = 7.088(1) Å; *V* = 1532.9(3) $Å^3$) was refined to an *R*1(*F*) value of 1.68 %. The eight strongest X-ray diffraction lines in the (calculated) powder pattern [*d* in Å(*I*)*hkl*] are: 2.5534(100)(051), 3.9508(85)(220), 2.9236(78)(122), 4.1783(61)(211), 2.4307(55)(012), 2.0198(39)(152), 1.8995(30)(342), 6.294(28)(101). The most common associated minerals are quartz, albite, microcline and apatite. Beryl and in places schorl are also found as primary pegmatitic phases. Because of the low mode of associated mica (muscovite), we assume that the silica melt, which formed this pegmatite, crystallized under relatively dry

conditions, in agreement with the observation that alumino-oxy-rossmanite contains a lower amount of OH than most other tourmalines. This new member of the tourmaline supergroup exhibits the most Al-rich end-member composition of the tourmaline supergroup (theoretical content: ~54 wt% Al_2O_3). The significant content of tetrahedrally-coordinated Al could reflect the relatively high-temperature conditions (~700 °C) inferred for crystallization of the pegmatite. Alumino-oxy-rossmanite was named for its chemical relationship to rossmanite, □$(LiAl_2)Al_6(Si_6O_{18})(BO_3)_3(OH)_3(OH)$, which in turn was named after Dr. George R. Rossman, Professor of Mineralogy at the California Institute of Technology (Pasadena, California, USA).

Key-words: Alumino-oxy-rossmanite, new mineral, Al-rich tourmaline, structure refinement, electron microprobe analysis, Moldanubian pegmatite, Eibenstein an der Thaya.

INTRODUCTION AND PREVIOUS WORK

The generalized formula of tourmaline-supergroup minerals can be written $XY_3Z_6(T_6O_{18})(BO_3)_3V_3W$, as proposed by Henry et al. (2011). These authors and Hawthorne (1996, 2002) suggest occupancies by the following most common cations:

$^{IX}X = Na^+, K^+, Ca^{2+}, □$ (vacancy)

$^{VI}Y = Fe^{2+}, Mg^{2+}, Mn^{2+}, Al^{3+}, Li^+, Fe^{3+}, Cr^{3+}, V^{3+}$

$^{VI}Z = Al^{3+}, Mg^{2+}, Fe^{3+}, Cr^{3+}, V^{3+}$

$^{IV}T = Si^{4+}, Al^{3+}, B^{3+}$

$^{III}B = B^{3+}$

$^{III}V = OH^-, O^{2-}$

$^{III}W = OH^-, F^-, O^{2-}$.

Some of these cations can be present simultaneously on two and even three structural sites, reflecting order-disorder phenomena, mainly between the octahedral Y- and Z-site occupants (Ertl et al. 2003 and references therein). The tourmaline supergroup comprises currently 38 valid mineral species accepted by the Commission on New Minerals, Nomenclature and Classification (CNMNC) of the International Mineralogical Association (IMA). They represent hydroxyl-, fluor- and oxy-species of X-site vacant, alkali and calcic tourmalines with typical octahedral occupants like Fe^{2+}, Mg^{2+}, Mn^{2+}, Al^{3+}, Li^{+}, Fe^{3+}, Cr^{3+}, and V^{3+} (Henry et al. 2011). Crystal-chemical relations in the tourmaline supergroup and the crystal chemistry of tourmaline-supergroup minerals have been investigated by many authors in the last 50 years (e.g., Donnay and Barton 1972, Povondra and Čech 1976, Deer et al. 1986, Foit 1989, Hawthorne et al. 1993, Hawthorne 1996, 2002, 2016, Henry and Dutrow 1996, Bloodaxe et al. 1999, Ertl et al. 2002, 2012a, 2012b, 2013, 2015, 2018, Hughes et al. 2011, Bosi and Lucchesi 2004, 2007, Bosi et al. 2004, 2013, 2015, 2017, Ertl and Tillmanns 2012, Ertl and Bačík 2020, Bačík and Fridrichová 2021). Tourmaline can also be a petrologic recorder of its geologic history as was demonstrated by Van Hinsberg et al. (2011).

Rossmanite, with the ideal end-member formula $\square(LiAl_2)Al_6(Si_6O_{18})(BO_3)_3(OH)_3(OH)$, is an alkali-deficient tourmaline that was described as a new tourmaline species from Rožná, western Moravia, Czech Republic, by Selway et al. (1998). “Oxy-rossmanite”, with the formula $\square(Li_{0.5}Al_{2.5})Al_6(Si_6O_{18})(BO_3)_3(OH)_3O$, was proposed as a hypothetical tourmaline end-member by Hawthorne and Henry (1999). This hypothetical tourmaline is characterized by a vacancy-dominated X site, an Al-dominated Y site (with a minor component of Li), and an O-dominated W site.

Here, we present the first natural occurrence of an even more aluminous end-member from Moldanubian pegmatites in Lower Austria. Additionally, we discuss the geological and petrological context of this unusual Al-rich tourmaline, which was recently given the new name alumino-oxy-rossmanite (IMA 2020-008b; Ertl et al. 2020). We also studied a second tourmaline sample (PINK2) of a more recent finding from this locality, since this tourmaline is close in composition to the holotype material of alumino-oxy-rossmanite (PINK1) in order to understand the significance of these Al-rich tourmalines.

SAMPLE DESCRIPTION AND TYPE MATERIAL

Tourmaline-bearing pegmatites from the western part of a quarry close to the village Eibenstein an der Thaya, Lower Austria, within the Moldanubian Drosendorf Unit with exposed marbles and amphibolites, were previously described by Götzinger et al. (1994). Subsequently, Ertl (1995) provided a more detailed description of these tourmalines. He characterized dravite, schorl and colored Al-rich tourmaline (pale blue, pink, dark green). The Al-rich tourmaline was originally assigned to Mn-/Fe-bearing olenite and elbaite, based on semiquantitative energy-dispersive X-ray spectroscopic analyses and the unit-cell parameters, which were in the range $a \approx$ 15.80–15.87 and $c \approx$ 7.09–7.10 Å. Ertl (1995) also characterized pale colored apatite, and beryl from the tourmaline-bearing pegmatite. Rare associated muscovite was also identified. Additional chemical, structural, and spectroscopic data of a pink tourmaline sample were given by Ertl et al. (2005). These authors demonstrated for the first time that it is possible to have significant amounts of both $^{[4]}$Al and $^{[4]}$B in an Al-rich tourmaline. They showed that this tourmaline has the highest known Al content of all natural tourmalines. Because of the dominant X-site vacancy, the O-dominant W site, and the Al-dominant Y site, this Mn- and Li-bearing tourmaline previously

was assigned to "oxy-rossmanite" (Ertl et al. 2005), a hypothetical end-member in the proposed classification of tourmalines (Hawthorne and Henry 1999). However, the Mn content was only determined as MnO_{total} and Li was calculated in the optimized formula for a fully occupied Y site without allowing any Y-site vacancies.

In 2017 another, small tourmaline-bearing pegmatite was briefly exposed in the northern part of the aforementioned quarry near Eibenstein. The mineralogy of this lenticular, deformed, but more or less concordant pegmatite was studied in detail by Kolitsch et al. (2020). The main components are quartz, microcline, and albite; mica (muscovite) were present only in trace amounts. Black, tectonically deformed and fractured schorl crystals up to 20 cm were embedded in the outer part of the pegmatite body, while a small central, coarse-grained area contained macroscopically grey-pink to dark pinkish, prismatic tourmalines, assigned to olenite (according to two crystal-structure refinements and analyses by using Scanning Electron Microscopy with Energy Dispersive Spectroscopy; Kolitsch et al. 2020). This pink tourmaline is generally overgrowing black to dark grey cores of Al-rich schorl, commonly with a narrow, pale to dark grey, smokey intermediate zone. The investigated olenitic tourmaline crystals exhibit lattice parameters of $a \approx 15.83$ and $c \approx 7.10$ Å (for additional structural and chemical data see Kolitsch et al. 2020). Some of the pink tourmaline crystals, which reached lengths up to 2.5 cm, were also tectonically deformed. They were bent, in part slightly broken and rehealed. Rarely, anhedral pink tourmaline fills very narrow (≤ 1 mm) cracks in black tourmaline or in feldspar, or very small interstitial voids in feldspar. Beryl, fluorapatite (partly Mn-bearing), rutile, and columbite-(Mn) are present as macroscopic accessories in this pegmatite. Further, mostly microscopic accessories (generally detected only in polished sections) include barite, bertrandite, bismuth,

eulytine, hübnerite, pezzottaite(?), pollucite, scheelite, stibarsen, titanite, „uranmicrolite", as well as several unidentified phases, including a new Cs-Al-phosphate.

When in 1994 a small pegmatitic body (WGS84 N 48°51'00" / E 015°34'55") was exposed in the aforementioned large quarry about 300 m NE of the village Eibenstein an der Thaya (often named Hengl quarry after the operator), only one tourmaline crystal, intimately intergrown with quartz, was found, which contained a pink core zone (~4 mm in diameter, ~4 mm in length; Figure 1) surrounded by a dark green rim. Parts of this pink tourmaline (now back in the collection of A.P.) were used as holotype material (sample PINK1). Recently in 2017, when another small pegmatitic body (WGS84 N 48°51'04" /E 015°34'57") was exposed, more pink tourmaline was found. This time the crystals had prismatic forms. A part of the pink tourmaline crystal shown in Figure 2 was also characterized (sample PINK2). The most common associated minerals of pink tourmaline in both pegmatites are quartz, albite, microcline and fluorapatite. Schorl was more common in the 1994 pegmatite. In this pegmatite (type locality) alumino-oxy-rossmanite was early in the magmatic crystallization history, especially in respect to other tourmalines. Schorl is overgrowing alumino-oxy-rossmanite while dravite (pale-green fibers) is the latest tourmaline in the crystallization sequence. The other magmatic phases quartz, albite, microcline and fluorapatite are more or less co-genetic to alumino-oxy-rossmanite.

Part of the holotype specimen of alumino-oxy-rossmanite (sample PINK1) was deposited as sample NMNH 173824 at the National Museum of Natural History, Smithsonian Institution, Washington DC, USA, as sample 134790 at the Mineralogical Museum, Harvard University, Cambridge, Massachusetts, USA, and as sample 93533 at the Fersman Mineralogical Museum, Moscow, Russia. A piece of the type specimen, which was sent to the California Institute of Technology for optical spectroscopy studies is designated GRR2170 (polished section).

REGIONAL GEOLOGY

The Moldanubian Zone as the south-eastern part of the Bohemian Massif consists of a thick crystalline complex and exposes medium- to high-grade metamorphic rocks with Paleoproterozoic to Devonian protolith ages (Sorger 2020). The results of a comprehensive P–T study by Soger (2020) along four W-E trending profiles revealed a different distribution of metamorphic conditions within the Drosendorf Unit, a nappe in the Moldanubian Zone in the Bohemian massif (Petrakakis 1997, Lindner et al. 2020); this unit comprises the host rocks of the tourmaline-bearing pegmatites. The complex is characterized by an interlayering of partly migmatitic, garnet- and sillimanite-bearing gneisses, quartzites, partially graphitic marbles and calc-silicate rocks, amphibolites and granitic orthogneisses. In general, a decreasing trend in metamorphic grade from SW to NE was observed. The Drosendorf Unit shows the highest temperature conditions of ~800 °C in the south and the lowest of 650 °C in the north (Sorger 2020). Metapelitic paragneisses, which are also the host rocks of the tourmaline-bearing pegmatites, from the southern Drosendorf Unit were affected by two metamorphic events. The first tectonothermal event of this unit was an early Variscan metamorphism in the Devonian at ~370 Ma. After an intermittent phase of cooling and exhumation, the Drosendorf was subjected to the predominant Variscan event in the Visean at ~340 Ma (Sorger 2020). While the first metamorphism was pressure dominated, exhibited the second metamorphose a relatively high geothermal gradient (Sorger 2020). In the Dosendorf Unit usually the second metamorphic event was the more significant regionally widespread metamorphism. Pegmatites around Eibenstein an der Thaya were formed during the pressure release of the predominant Variscan event in the Visean at ~340 Ma, e.g., a pegmatite containing tourmaline, topaz and cassiterite dated at 337±5 Ma from a Sm-Nd garnet-albite isochron (Ertl et al. 2004). Low H_2O activities during the second

event might be a consequence of aqueous fluid being driven off, which might have started already during the early Variscan metamorphism in the Devonian at ~370 Ma.

The pegmatitic body in which the new Al-rich tourmaline was found, was found in amphibolite and biotite paragneiss in the Drosendorf window. The Variscan metamorphic conditions for the Moldanubian rocks for this area of the Drosendorf nappe system are described as 0.4-0.8 GPa / 680-750 °C (calculated by using pseudosections; Sorger 2020). Based on a map of that area contoured for temperature and pressure (Figure 2.3, Sorger 2020) the metamorphic P-T conditions during the predominant Variscan event for the Moldanubian rocks in the Hengl quarry, at the time when the pegmatites intruded, were ~0.6 GPa / ~700 °C. Several pegmatitic bodies occurred as vertically extended lenses with dimensions of up to ~5 × 3 m and a thickness of up to ~50 cm. Each lens included up to ~5 m^3 coarse-grained pegmatitic rock. The pegmatites show a relatively sharp contact to their host rocks. Pegmatites hosted by a fine-grained biotite-rich paragneiss have a relatively sharp contact and a narrow chilled margin zone. Fine-grained black tourmaline in the intersection between pegmatite and host rock suggests that there had been some interaction between them.

MATERIALS AND METHODS

Chemical analyses

The two crystal fragments selected for crystal-structure determination (PINK1, from the 1994 pegmatite, and PINK2, from the 2017 pegmatite) were embedded in epoxy on a single 2.5 cm diameter round glass slide and polished. All elements reported here except B, Li, Be, and H were determined with a Cameca SX51 electron microprobe (EMP) equipped with five wavelength-dispersive spectrometers (Universität Heidelberg). Operating conditions: 15 kV

205 accelerating voltage, 20 nA beam current, and beam diameter 5 μm. Peaks for all elements were
206 measured for 10 s, except for Mg (20 s), Ti (20 s), Zn (30 s), and F (40 s). We used the following
207 (natural and synthetic) reference materals and X-ray lines for calibration: topaz (F*K*α), albite
208 (Na*K*α), wollastonite (Si*K*α) and (Ca*K*α), corundum (Al*K*α), periclase (Mg*K*α), orthoclase (K*K*α),
209 rutile (Ti*K*α), rhodonite (Mn*K*α), hematite (Fe*K*α), and gahnite (Zn*K*α). The analytical data were
210 reduced and corrected using the PAP routine (Pouchou and Pichoir 1991). A modified matrix
211 correction was applied assuming stoichiometric O atoms and all non-measured components as
212 B_2O_3. The accuracy of the electron-microprobe analyses and the correction procedure was
213 checked by measuring three samples of reference tourmalines (98114: elbaite, 108796: dravite,
214 112566: schorl). Compositions of these tourmaline samples were determined as part of an
215 interlaboratory comparative study (Dyar et al. 1998, 2001). Under the described conditions, the
216 accuracy of all analyses is ± 1% relative for major elements and ± 5% relative for minor
217 elements.

218 H, Li, and B were determined in PINK2 by SIMS with a CAMECA ims 3f ion
219 microprobe (Universität Heidelberg). Primary O^- ions were accelerated to 10 keV. The mass
220 spectrometer's energy window width was 40 eV. An offset of 75 V was applied to the secondary
221 accelerating voltage of 4.5 kV so that secondary ions with an initial energy of 75 ± 20 eV were
222 analyzed (energy filtering), which minimizes potential matrix effects (Ottolini et al. 1993). The
223 primary current was 10 nA, resulting in a spot diameter of ~20 μm. The spectrometer's mass
224 resolving power (MRP) M/ΔM for B, Li and Si was set to ~1000 (10%) to suppress interferences
225 ($^6LiH^+$, $^{10}BH^+$, Al^{3+}). Secondary ^7Li, ^{11}B and ^{30}Si ions were collected under an imaged field of
226 150 μm diameter. For H (and Si) the MRP M/ΔM was set to ~400 (10%) and the imaged field
227 was limited to a diameter of ~12 μm. In-situ water contamination was reduced by using a liquid

nitrogen cold-trap attached to the sample chamber (Ludwig and Stalder 2007, and references therein). The count rates of the analyzed isotopes (^{1}H, ^{7}Li and ^{11}B) were normalized to the count rate of ^{30}Si and relative ion yields (RIY) were used for quantification of the results (*e.g.*, Hinton 1990, 1995, Ottolini et al. 1993). The analytical procedures for the SIMS analyses (which included Be) of sample PINK1 were almost identical (details see Ertl et al. 2005).

The relative ion yields for H and B were determined using three tourmalines as reference material: elbaite, dravite and schorl (Dyar et al. 1998, 2001). The reference material for Li and Be was the NIST SRM610 standard glass with concentrations for Li (464.2 μg g^{-1}) and Be (469.0 μg g^{-1}) average taken from Pearce et al. (1997). The relative reproducibility (1σ) for the RIY of H, Li, Be and B was <1%. Matrix effects and the uncertainty of the element concentrations in the reference material limit the accuracy of the analysis. The relative accuracy is estimated to be <20% for H and <10% for Li, Be and B. Table 1 contains complete chemical analyses of the two studied crystal fragments of pink Al-rich tourmaline.

Powder X-ray diffraction

The eight strongest X-ray diffraction lines in the (calculated) powder pattern [*d* in Å(*I*)*hkl*] are: 2.5534(100)(051), 3.9508(85)(220), 2.9236(78)(122), 4.1783(61)(211), 2.4307(55)(012), 2.0198(39)(152), 1.8995(30)(342), 6.294(28)(101) (Supplementary Table S1). The X-ray powder diffraction pattern had to be calculated because only a very small amount of material was available for scientific studies of the single small pink tourmaline crystal, which was originally found in 1994. Although pink tourmaline was found more frequently in the 2017 pegmatite, the chemistry of the studied crystals was not as close to the ideal end-member as that of the 1994 material.

Crystal-structure refinement

A fragment of the holotype crystal (PINK1) was mounted on a Bruker Apex CCD X-ray diffractometer equipped with graphite-monochromatized Mo*K*α radiation (Department of Geology, Miami University, Oxford, Ohio, U.S.A.). Redundant data were collected for an approximate sphere of reciprocal space, and were integrated and corrected for Lorentz and polarization factors, and for absorption, using the Bruker program SAINTPLUS (Bruker AXS Inc. 2001). The structure was refined with the Bruker SHELXTL V. 6.10 package of programs, with neutral-atom scattering factors and terms for anomalous dispersion.

A fragment of PINK2 was structurally investigated at the Institut für Mineralogie und Kristallographie, Geozentrum, Universität Wien, Austria. As a first step, the quality of different crystal fragments was checked with a Bruker APEXII diffractometer equipped with a CCD area detector and an Incoatec Microfocus Source IμS (30 W, multilayer mirror, Mo*K*α). The crystal with the best diffracting quality was subsequently measured on this diffractometer. Single-crystal X-ray diffraction intensity data, up to 82.84° 2θ, were collected at room temperature, integrated, and corrected for Lorentz and polarization factors, and with a multi-scan absorption correction (Sheldrick 2002). The structure was refined with SHELXL-97 (Sheldrick 2008) using scattering factors for neutral atoms.

The refinements were performed with anisotropic displacement parameters for all non-hydrogen atoms. The various site occupancies were refined according to well-known characteristics of the tourmaline structure (Henry et al. 2011), and considering the results of the EMP, SIMS, and spectroscopic analyses. Hence, the X site occupancy was refined using a Na scattering factor, the Y site with Al and Li scattering factors, the T site with Si and B, and the Al

occupancy at the Z site was fixed at 1.00, typical for Al-rich tourmalines. The W site was preliminarily refined with O *vs* F scattering factors, but because the resulting value for F was lower than the standard deviation, in the final cycles the W site was only refined with O scattering factors.

Refined unit-cell parameters and the most important average bond lengths for PINK1 and PINK2 are listed in Table 2. Supplementary Material (CIF) provides crystal data and details of both structure refinements (atomic coordinates, individual bond lengths and angles).

Optical spectroscopy

A 380 × 185 μm^2 crystal fragment of the holotype PINK1 was prepared as a 92.8 μm thick parallel plate polished on both sides to study its color properties. Polarized optical absorption spectra in the 390-1100 nm range were obtained at about one nm resolution with a locally-built microspectrometer system consisting of a 1024-element Si diode-array detector coupled to a grating spectrometer system *via* fiber optics to a highly-modified NicPlan® infrared microscope containing a calcite polarizer. A pair of conventional 10x objectives was used as an objective and a condenser. Spectra were obtained through the central area of the sample, which included a veil of two-phase (liquid/gas) inclusions.

Infrared spectra

Infrared spectra of holotype material to examine the OH content were measured in the main compartment of a Nicolet Magna 860 FTIR spectrometer at 2 cm^{-1} resolution using a 200 μm aperture. Near-IR spectra were obtained using a CaF_2 beam splitter, tungsten-halogen source, MCT-A detector, and $LiIO_3$ polarizer, and were averaged over 256 to 4000 scans. For the

297 smallest crystal fragments, a silica beam splitter and InSb detector were used to collect the
298 spectra. Additional spectra were obtained with a Nicolet Continuum infrared microscope using a
299 MCT-A/CaF_2/tungsten-halogen combination.

300 The total integrated band area ($area_{tot} = area_{E\|c} + 2 \times area_{E\perp c}$) was determined for the mid-
301 IR OH overtone bands using Omnic E.S.P. 5.2 software. Integrated absorbances were determined
302 by establishing a suitable baseline and measuring the area between the curve and the baseline
303 over the region of the OH bands. The baseline connects with the spectral trace on both the high-
304 and low-energy side of the OH region. This was done on a spectrum normalized for a 1-cm-thick
305 crystal. Before integration, a minor, visually estimated, background correction was needed to
306 compensate for a sloping background.
307

308 ## RESULTS AND DISCUSSION

309

310 ### Physical properties

311 Holotype alumino-oxy-rossmanite is brittle and has a Mohs hardness of 7; it is non-
312 fluorescent, has no observable parting and cleavage, and has a vitreous luster. The megascopic
313 color of alumino-oxy-rossmanite is pink and the streak is white. It has a measured density of
314 3.07(3) g/cm^3 (pycnometer method; Syromyatnikov 1935, Ksanda and Merwin 1939) and a
315 calculated density of 3.092(1) g/cm^3 based on the empirical formula and the unit-cell volume
316 refined from the single-crystal X-ray diffraction data. The fracture is conchoidal. The mineral has
317 a prismatic habit, but only crude prismatic forms are developed. Twinning was not observed.
318

319 ### Optical spectroscopy and optical properties

The optical absorption spectrum of alumino-oxy-rossmanite (Fig. 3) is most intense in the E⊥c direction. It consists of a band at about 555 nm and weaker features near 450 and 415 nm. The E||c spectrum also contains the 555 nm band that overlaps with another broad band near 475 nm. There is also an indication of a weak band near 780 nm. The broad rise in absorption from high- to low-energy could be due in part to scattering from imperfections in the crystal, and partly to an ultraviolet absorption band. The spectrum is broadly similar to the spectrum of rossmanite (Ertl et al. 2005), but the major bands are shifted to longer wavelengths. For example, in rossmanite, the main band is observed at 517 nm.

The pink color of alumino-oxy-rossmanite is due to the band at 555 nm that is associated with Mn^{3+} probably produced by natural irradiation of Mn^{2+} as has been previously described for elbaite (Reinitz and Rossman 1988). In plane-polarized light, alumino-oxy-rossmanite is pleochroic, O = pink, E = near-colorless (polarized parallel to the c-axis; orientation: E || *c*). Alumino-oxy-rossmanite is uniaxial negative, ω = 1.648(5), ε = 1.628(5) (590 nm).

Infrared spectroscopy

The infrared spectrum obtained in the mid-infrared region (Fig. 4) of sample PINK1 shows OH bands in the E||c spectrum at 7175, 7144, 7022, ~6964 cm^{-1}, and the most prominent band at 6708 cm^{-1}. These bands are shifted to lower wavenumbers as compared to the corresponding bands in fluor-elbaite of similar divalent-cation composition (Ertl et al. 2015). Mattson (1985) concluded that the 7001 cm^{-1} band in an elbaitic tourmaline (sample GRR 598-Afgh-1) is associated with H bound to the O3 site with a local configuration involving Li^{+}. This band is of low intensity in alumino-oxy-rossmanite compared to the elbaitic tourmaline of Mattson (1985). The low intensity of these OH bands suggests that the absolute OH concentration

343 is lower than that in sample GRR 598-Afgh-1. Because no absolute calibration of the intensity of
344 the OH overtone bands in the tourmaline spectrum has yet been done, it is not possible at this
345 time to establish an absolute concentration. By comparing the OH intensity of alumino-oxy-
346 rossmanite to other relevant tourmalines (twenty-five elbaites, fluor-elbaites, fluor-liddicoatites,
347 and rossmanites), alumino-oxy-rossmanite remains the tourmaline with integrated intensity that is
348 signifiantly lower than all the other tourmaline samples (Ertl et al. 2015). All of these
349 observations are highly suggestive that alumino-oxy-rossmanite contains a lower amount of OH
350 than most other tourmalines. The infrared spectrum confirms that hydroxyl groups in holotype
351 alumino-oxy-rossmanite (sample PINK1) are present at a lower concentration than commonly
352 found in other Li-bearing tourmalines.
353 By applying the Beer's Law epsilon value (estimated to be 7.5 for Mn^{3+}; Reinitz and
354 Rossman 1988) to the optical absorption spectrum (Fig. 2) and by determination of the Mn^{3+}
355 band heights, considering the chemistry and the density (3.09) of alumino-oxy-rossmanite, we
356 were able to estimate the percentage of Mn, which was oxidized to Mn^{3+} (~74%). Because iron is
357 oxidized under less oxidizing conditions than manganese, which is shown in Figure 3 of Huebner
358 (1969), we consider the percentage of the oxidized Fe to be similar, if not higher than it is for
359 Mn. It is not uncommon that the small amount of total Fe in pink Al-rich and Li-bearing
360 tourmalines is oxidized to a relatively high percentage (~60-90% as determined by Mössbauer
361 spectroscopy; Ertl et al. 2010). The oxidation of relatively high amounts of Mn and Fe in
362 alumino-oxy-rossmanite is in agreement with the observation that the OH groups are present at a
363 lower concentration than commonly found in other Al-rich and Li-bearing tourmalines.

This is the peer-reviewed, final accepted version for American Mineralogist, published by the Mineralogical Society of America.
The published version is subject to change. Cite as Authors (Year) Title. American Mineralogist, in press.
DOI: https://doi.org/10.2138/am-2022-8047. http://www.minsocam.org/

Crystal structure

The crystal structure of alumino-oxy-rossmanite (holotype material, sample PINK1; space group $R3m$; a = 15.803(1), c = 7.088(1) Å; V = 1532.8(3) Å^3) was refined to an $R1(F)$ value of 1.68 %. The crystal structure of tourmaline sample PINK2 (a = 15.809(1), c = 7.082(1) Å; V = 1532.9(3) Å^3) was refined to an $R1(F)$ value of 1.37 %. The empirical formulae of these samples were determined on the basis of EMPA, SIMS, spectroscopical methods (optical absorption and infrared spectroscopy), and SREF as follows:

PINK1: $^{X}(\square_{0.53}Na_{0.46}Ca_{0.01})\ ^{Y}(Al_{2.37}Mn^{3+}_{0.21}Li_{0.16}\square_{0.14}Mn^{2+}_{0.07}Fe^{3+}_{0.03}Fe^{2+}_{0.01}Ti^{4+}_{0.01})\ ^{Z}Al_6$ $(Si_{5.37}Al_{0.41}B_{0.22}O_{18})(BO_3)_3\ ^{V}[(OH)_{2.77}O_{0.23}]\ ^{W}[O_{0.80}(OH)_{0.15}F_{0.05}]$.

PINK2: $^{X}(Na_{0.56}\square_{0.42}Ca_{0.02})\ ^{Y}(Al_{2.18}Li_{0.29}Mn^{3+}_{0.23}\square_{0.19}Mn^{2+}_{0.08}Ti^{4+}_{0.02}Fe^{3+}_{0.01})\ ^{Z}Al_6$ $(Si_{5.35}Al_{0.34}B_{0.31}O_{18})(BO_3)_3\ ^{V}[(OH)_{2.90}O_{0.10}]\ ^{W}[O_{0.63}F_{0.21}(OH)_{0.16}]$.

No H could be found at the W site (O1 site) by refinement, and also the difference-Fourier map around the W site indicates this site to be mainly occupied by O. The map shows a spherical electron density similar to that described by Cámara et al. (2002) [Fig. 1a of that paper, crystal 1, dravite, with 0.18 (OH) at the W site]. Because of a small, but still visible OH1 band in the IR spectrum, only 0.15 (OH) *pfu* have therefore been assigned to the W site. Ertl et al. (2002) showed that the bond-angle distortion (σ_{oct}^2) of the ZO_6 octahedron in a tourmaline is largely a function of the <Y-O> distance of that tourmaline, although the occupant of the O3 site (V site) also affects that distortion. For all investigated tourmalines in which the V site is completely occupied by 3 (OH) groups, including the samples from Hughes et al. (2004), the covariance, r, of <Y-O> and the σ_{oct}^2 of the ZO_6 octahedron is -0.991 (Fig. 5). In Figure 5 the data of the

holotype material (PINK1) of alumino-oxy-rossmanite lies between the tourmalines that contain 3 (OH) at the V site and natural fluor-buergerite, which contains 0.3 (OH) and 2.7 O at the V site. In addition, tourmaline sample PINK2 is slightly shifted in the direction of OH-poor fluor-buergerite. The calculated wt% for H_2O is ~14% lower than the measured value (by SIMS) for sample PINK2. One possible explanation for the higher value as obtained by SIMS is that alumino-oxy-rossmanite contains H_2O-bearing fluid inclusions (Ertl et al. 2005). However, these errors are still lower than the relative uncertainty of the SIMS analyses.

The structural refinement of the X site of the type material (PINK1) confirms an occupancy of Na <50% (only very small amounts of Ca were found by chemical analyses; Table 1). Only Al was found to occupy the Z site and also the refined Y-site occupancies are in good agreement with the chemistry (Table 1). Although the structure refinements show significant amounts of $^{[4]}$B (0.28(1) - 0.33(2) apfu), the <T-O> bond-lengths are in the range 1.617(1) - 1.619(1) Å (Table 2), which is, within the standard deviation, close to a T site fully occupied with Si (McDonald and Hawthorne 1995, Bloodaxe et al. 1999, Bosi et al. 2005). Because of a relatively low Si content in both samples (~5.4 apfu Si; Table 1), these bond-lengths can only be explained by significant amounts of $^{[4]}$Al in addition to $^{[4]}$B. A substitution of Si by Al in tourmaline was described for the first time by Foit and Rosenberg (1979). The type material of alumino-oxy-rossmanite (sample PINK1) contains 0.41 apfu $^{[4]}Al^{3+}$. The simplified T-site occupation can also be written as $(R^{4+}{}_5R^{3+})$ or as $[Si^{4+}{}_5(Al,B)^{3+}]$. Hence, alumino-oxy-rossmanite is an Al-rich tourmaline that contains not only Si, but also significant amounts of B and Al at the T site. Elbaitic and olenitic tourmaline samples from pegmatites often contain $^{[4]}$B as well as $^{[4]}$Al (Ertl et al. 2007, 2009, 2010, Lussier et al. 2009).

The lattice parameters of both investigated samples are among the lowest observed among natural tourmalines, also lower than other samples from this locality (Kolitsch et al. 2020). Alumino-oxy-rossmanite has the highest known Al content of all natural tourmalines (up to 47.08 wt% Al_2O_3; up to 8.78 apfu Al). Very high Al contents were also found in colorless olenite from Koralpe, Styria, Austria (up to 46.53-46.71 wt% Al_2O_3 and 8.46 apfu Al; Ertl et al. 1997, Hughes et al. 2000), and in olenite from the type locality Olenii Range, Voron'í Tundry, Kola Peninsula, Russia (up to 45.79-46.43 wt% Al_2O_3 and 8.52 apfu Al; Sokolov et al. 1986, Schreyer et al. 2002). Every tourmaline can be described very well by the mol% of different endmembers, like every garnet. Considering the end-member formula of alumino-oxy-rossmanite (see next section), the major components of sample PINK1 (holotype material) are 41 mol% alumino-oxy-rossmanite, 33 mol% olenite, and 9 mol% elbaitic tourmaline (fluor-elbaite, elbaite). The sum of these components is 83 mol%. The major components of sample PINK2 are 34 mol% alumino-oxy-rossmanite, 28 mol% olenite, and 19 mol% elbaitic tourmaline and hence this sample is a complex intergrowth of different endmembers, mainly of the alumino-oxy-rossmanite – olenite solid solution. The sum of these components is 81 mol%. Minor components in both samples are fluor-liddicoatite and tsilaisite with ≤ 3 mol%. The rest of the cations cannot yet be assigned to a special tourmaline, because there is no end-member established which includes Mn^{3+} or ^{T}B. We conclude that in both samples alumino-oxy-rossmanite is the dominant component. In contrast to PINK1, sample PINK2 is characterized by a lower alumino-oxy-rossmanite component and a higher elbaitic component.

Endmember formula and relationship to other tourmalines

The empirical formula of the holotype material, calculated on the basis of 31(O,OH,F), is $^{X}(\square_{0.53}Na_{0.46}Ca_{0.01})\ ^{Y}(Al_{2.37}Mn^{3+}_{0.21}Li_{0.16}\square_{0.14}Mn^{2+}_{0.07}Fe^{3+}_{0.03}Fe^{2+}_{0.01}Ti^{4+}_{0.01})\ ^{Z}Al_6(BO_3)_3(Si_{5.37}Al_{0.41}B_{0.22}O_{18})\ ^{V}[(OH)_{2.77}O_{0.23}]\ ^{W}[O_{0.80}(OH)_{0.15}F_{0.05}]$.

Details of the occupation of both (OH)/O sites are given in the Crystal structure section above. The simplified formula is $(\square,Na)(Al,Mn,Li,\square)_3Al_6(BO_3)_3[(Si,Al,B)_6O_{18}][(OH),O]_3[O,(OH)]$. When applying the IMA-CNMNC recommended use of the dominant-valency rule for tourmaline-supergroup minerals, the Y-site cations are ordered as follows: $(Al,Mn,Fe)^{3+}_{2.6} > (Li)^{+}_{0.2} > (Mn,Fe)^{2+}_{0.1}$, that is $R^{3+}_{2.6} > R^{+}_{0.2} > R^{2+}_{0.1}$. Hence, our new tourmaline corresponds to the "X-site vacant tourmaline group" (Henry et al. 2011). The most abundant cation at the Y site with the charge 3+ is aluminum: $Al^{3+}_{2.4} > Mn^{3+}_{0.2} > Fe^{3+}_{<0.1}$.

If we use the empirical formula and apply the site total charge approach (Bosi et al. 2019), which is useful for identifying new tourmaline endmembers, two configurations are possible:

1) Y = +8 and T = +24;

2) Y = +9 and T = +23.

In accord with the chemical composition of the Y and T sites of the studied sample, the possible atomic arrangements are quantitatively evaluated in terms of apfu as follows:

Configuration 1:

a) $^{Y}(R^{3+}_{2}R^{2+})^{\Sigma 8+}\ ^{T}(R^{4+}_{6})^{\Sigma 24+} = {}^{Y}(R^{3+}_{2}R^{2+})_{0.08}\ ^{T}(R^{4+}_{6})_{0.08} = {}^{Y}(Al^{3+}_{0.16}R^{2+}_{0.08})\ ^{T}(Si^{4+}_{0.48}) = 0.72$ apfu, limited by the R^{2+} content;

b) $^{Y}(R^{3+}_{2.5}R^{+}_{0.5})^{\Sigma 8+}\ ^{T}(R^{4+}_{6})^{\Sigma 24+} = {}^{Y}(R^{3+}_{2.5}R^{+}_{0.5})_{0.32}\ ^{T}(R^{4+}_{6})_{0.32} = {}^{Y}(Al^{3+}_{0.80}Li^{+}_{0.16})\ ^{T}(Si^{4+}_{1.92}) = 2.88$ apfu, limited by the Li content.

This is the peer-reviewed, final accepted version for American Mineralogist, published by the Mineralogical Society of America.
The published version is subject to change. Cite as Authors (Year) Title. American Mineralogist, in press.
DOI: https://doi.org/10.2138/am-2022-8047. http://www.minsocam.org/

c) $^{Y}(R^{3+}_{8/3}\square_{1/3})^{\Sigma 8+}\ ^{T}(R^{4+}_{6})^{\Sigma 24+} = {}^{Y}(R^{3+}_{8/3}\square_{1/3})_{0.42}\ ^{T}(R^{4+}_{6})_{0.42} = {}^{Y}(Al^{3+}_{1.12}\square_{0.14})\ ^{T}(Si^{4+}_{2.52}) = 3.78$ apfu, limited by the number of vacancies.

Configuration 2:

Only the following end-member charge arrangement is in agreement with configuration 2:

$^{X}\square\ ^{Y}(R^{3+}_{3})^{\Sigma 9+}\ ^{Z}Al_6\ [^{T}(R^{4+}_{5}R^{3+})^{\Sigma 23+}O_{18}](BO_3)_3\ ^{V}(OH)_3\ ^{W}O$.

In the studied sample, the arrangement compatible with the Y-site and T-site constituents are: $^{Y}(R^{3+}_{3})^{\Sigma 9+}\ ^{T}(R^{4+}_{5}R^{3+})^{\Sigma 23+} = {}^{Y}(R^{3+}_{3})_{0.87}\ ^{T}(R^{4+}_{5}R^{3+})_{0.87} = {}^{Y}(Al^{3+}_{2.61})\ ^{T}(Si^{4+}_{4.35}R^{3+}_{0.87}) = 7.83$ apfu, limited by $^{T}R^{3+}$ contents. Actually, this arrangement is limited by the □ content at the X site (0.53 vacancies pfu), and consequently the actual number of atoms decreases to 4.77 apfu. We assume that the measured contents of B and Li are reasonably accurate, because the excess B (B > 3.00 apfu) as well as the Li content are relatively small. Hence, we conclude that $^{T}Al > {}^{T}B$. When we use the empirical formula, the amount of the end-member charge arrangement of configuration 2 is the largest one, and since $^{T}Al > {}^{T}B$, the end-member formula of the studied sample can be written as $\square Al_3Al_6(BO_3)_3(Si_5AlO_{18})(OH)_3O$. This ideal formula requires SiO_2 31.90, Al_2O_3 54.14, B_2O_3 11.09, H_2O 2.87, total 100 wt%.

Hawthorne and Henry (1999) were the first to propose "oxy-rossmanite", with the ideal formula $\square(Li_{0.5}Al_{2.5})Al_6(Si_6O_{18})(BO_3)_3(OH)_3O$, as a hypothetical tourmaline end-member, because of its relationship to rossmanite (Selway et al. 1998). While rossmanite contains an (OH) at the W site, "oxy-rossmanite" contains an oxygen (O^{2-}) at this site. Because the new tourmaline contains not only more Al, which fills the Y and Z sites entirely and the Si site partially, than "oxy-rossmanite", but also O^{2-} at the W site, we suggest the name alumino-oxy-rossmanite, with

476 the end-member formula □$Al_3Al_6(BO_3)_3(Si_5AlO_{18})(OH)_3O$. Alumino-oxy-rossmanite is named
477 for its chemical relationship to rossmanite, □$(LiAl_2)Al_6(Si_6O_{18})(BO_3)_3(OH)_3(OH)$, which in turn
478 was named after Dr. George R. Rossman, Professor of Mineralogy at the California Institute of
479 Technology (Pasadena, California, USA). With the proposed name it is evident how this end-
480 member is related to the quite common tourmaline rossmanite and to "oxy-rossmanite". We also
481 want to keep the tourmaline nomenclature as simple as possible so that the name already gives
482 some information about the composition.

483 How the theoretical chemical composition of alumino-oxy-rossmanite is related to the
484 tourmalines rossmanite, "oxy-rossmanite", elbaite, fluor-elbaite, darrellhenryite, olenite, fluor-
485 liddicoatite, and liddicoatite is shown in Supplemental Table S2. For further comparison,
486 chemical analyses and selected physical properties of the valid species of Li-bearing tourmaline
487 end-members of the tourmaline supergroup (Henry et al. 2011) are given in Table 3. The
488 comparison shows that alumino-oxy-rossmanite and rossmanite have the smallest unit-cell
489 parameters of all these species. The derivation of alumino-oxy-rossmanite from rossmanite
490 appears to be a two-step process as shown in plots in Figures 6 and 7. The second step involves
491 the T sites, which is unique to alumino-oxy-rossmanite among tourmalines. For example, $^{Y}Li_{0.5}$ +
492 ^{V}OH in rossmanite = $^{Y}Al_{0.5}$ + ^{V}O in "oxy-rossmanite" while Si remains equal to 6. In contrast,
493 $^{Y}Al_{0.5}$ + ^{T}Al in alumino-oxy-rossmanite = $^{Y}Li_{0.5}$ + ^{T}Si in "oxy-rossmanite", that is, the T site is
494 involved. Ignoring the changes in Si occupancy results in the two analyzed tourmaline samples
495 (PINK1 and PINK2) plotting between endmember "oxy-rossmanite" and endmember olenite and
496 not between endmember alumino-oxy-rossmanite and endmember "oxy-rossmanite". This
497 omission is overcome by having two plots side-by-side (see Figures 6 and 7).
498

This is the peer-reviewed, final accepted version for American Mineralogist, published by the Mineralogical Society of America.
The published version is subject to change. Cite as Authors (Year) Title. American Mineralogist, in press.
DOI: https://doi.org/10.2138/am-2022-8047. http://www.minsocam.org/

IMPLICATIONS

The new tourmaline alumino-oxy-rossmanite represents the most Al-rich end-member composition of all tourmalines. Because the six-coordinated sites were mainly occupied by Al^{3+}, other sites must have appropriate charges to produce a charge-balanced formula. The choices are cation vacancies at the X site, trivalent cations at the T site, and an O-for-OH substitution at the OH sites. We have learned in our study, that all three of these possibilities are observed in alumino-oxy-rossmanite. The tourmaline structure seems to be flexible enough for Al to occupy not only the Y and Z sites simultaneously, but also to occupy part of the T site. A T-site occupancy with (Si_5Al), as was written in the theoretical end-member formula of alumino-oxy-rossmanite, seems to mark the highest possible amount of Al that can be included at this site (see also Ertl et al. 2018).

Tetrahedrally-coordinated B increases with decreasing temperature at pressures below pressures of ~1000–1500 MPa (Ertl et al. 2008, 2012a, 2018). In contrast, $^{[4]}$Al often increases with increasing temperature (Henry and Dutrow 1996). A possible explanation for the observation that $^{[4]}Al > {}^{[4]}B$ in this early-magmatic tourmaline, could be that Al^{3+} is favored by the relatively high-temperature conditions of ~700 °C (Sorger 2020) during formation of these Moldanubian pegmatites. Alumino-oxy-rossmanite contains up to ~0.4 apfu $^{[4]}$Al. It is not uncommon for high-grade metamorphic rocks (upper-amphibolite to granulite-facies) to contain tourmaline with up to 0.4 apfu $^{[4]}$Al (e.g. Grew et al. 1990, 1997, Henry and Dutrow 1996). This is also in agreement with another Al-rich oxy-tourmaline with tetrahedrally-coordinated Al from small bodies of abyssal pegmatite located in the eastern part of the Moldanubian Zone, Bohemian Massif, Czech Republic (Cempírek et al. 2006).

Alumino-oxy-rossmanite was formed during relatively dry conditions of the pegmatitic melt, reflected by the low quantity of associated mica (muscovite) and the occurrence of oxy-

523 tourmalines, which are linked to low aH_2O. Although the amount of muscovite also depends on
524 the availability of Al, which would appear to be relatively high given the tourmaline composition,
525 it is possible that it in turn could reflect high B with tourmaline sequestering the Al and thereby
526 prohibiting other aluminous minerals from forming (Hinsberg and Schumacher 2007).

527 A major implication of such a temperature-sensitive T-site occupancy could be the
528 development of a geothermometer. More investigations of tourmaline in petrologically well-
529 characterized rocks and synthesis experiments are necessary for the exact understanding of the
530 temperature dependence of the tourmaline T-site occupancy. We conclude that, in our opinion,
531 the presence of alumino-oxy-rossmanite is indicative of high-temperature conditions in a
532 relatively dry environment, which is poor in Li and F.

533

534 **ACKNOWLEDGEMENTS**

535 We thank Andreas Wagner, University of Vienna, Austria, for preparing the tourmaline
536 samples. We are also thankful to Ralf Schuster and Manfred Linner, both from the Geological
537 Survey of Austria (Vienna), and to Gerlinde Habler (Department of Lithospheric Research,
538 Vienna), for helpful discussions and references. The constructive comments from Associate
539 Editor Edward S. Grew (University of Maine, Orono), as well as from reviewers Vincent van
540 Hinsberg (McGill University, Montreal) and Peter Bačík (Comenius University, Bratislava) were
541 very helpful to improve this work. This study was supported by the Austrian Science Fund
542 (FWF) project no. P 31049-N29 (AE).

543

544 **REFERENCES CITED**

545 Bačík, P. and Fridrichová, J. (2021) Cation partitioning among crystallographic sites based on
546 bond-length constraints in tourmaline-supergroup minerals. American Mineralogist, in press.
547 DOI 10.2138/am-2021-7804.
548 Bloodaxe, E.S., Hughes, J.M., Dyar, M.D., Grew, E.S., and Guidotti, C.V. (1999) Linking
549 structure and chemistry in the schorl-dravite series. American Mineralogist, 84, 922–928.
550 Bosi, F. and Lucchesi, S. (2004) Crystal chemistry of the schorl-dravite series. European Journal
551 of Mineralogy, 16, 335–344.
552 Bosi, F. and Lucchesi, S. (2007) Crystal chemical relationships in the tourmaline group:
553 structural constraints on chemical variability. American Mineralogist, 92, 1054–1063.
554 Bosi, F., Lucchesi, S., and Reznitskii, L. (2004) Crystal chemistry of the dravite-chromdravite
555 series. European Journal of Mineralogy, 16, 345–352.
556 Bosi, F., Andreozzi, G.B., Federico, M., Graziani, G., and Lucchesi, S. (2005) Crystal chemistry
557 of the elbaite-schorl series. American Mineralogist, 90, 1784–1792.
558 Bosi, F., Skogby, H., Hålenius, U., and Reznitskii, L. (2013) Crystallographic and spectroscopic
559 characterization of Fe-bearing chromo-alumino-povondraite and its relations with oxy-
560 chromium-dravite and oxy-dravite. American Mineralogist, 98, 1557–1564.
561 Bosi, F., Andreozzi, G.B., Hålenius, U., and Skogby, H. (2015) Experimental evidence for partial
562 Fe^{2+} disorder at the Y and Z sites of tourmaline: a combined EMP, SREF, MS, IR and OAS
563 study of schorl. Mineralogical Magazine, 79, 515–528.
564 Bosi, F., Cámara, F., Ciriotti, M.E., Hålenius, U., Reznitskii, L., and Stagno, V. (2017) Crystal
565 chemical relations and classification problems of tourmalines belonging to the oxy-schorl–
566 oxy-dravite–bosiite–povondraite series. European Journal of Mineralogy, 29, 445–455.
567 Bosi, F., Biagioni, C., and Oberti, R. (2019) On the chemical identification and classification of
568 minerals. Minerals, 9, 591.

569 Cámara, F., Ottolini, L., and Hawthorne, F.C. (2002) Chemistry of three tourmalines by SREF,
570 EMPA, and SIMS. American Mineralogist, 87, 1437–1442.
571 Cempírek, J., Novák, M., Ertl, A., Hughes, J.M., Rossman, G.R., and Dyar, M.D. (2006) Fe-
572 bearing olenite with tetrahedrally coordinated Al from an abyssal pegmatite of the Bohemian
573 massif at Kutná Hora: Structure, crystal chemistry, and optical spectra. Canadian Mineralogist,
574 44, 23–30.
575 Deer, W.A., Howie, R.A., and Zussman, J. (1986) Rock-forming minerals. Vol. 1B: Disilicates
576 and ring silicates, 2nd ed., Longman, Burnt Mill, Harlow, England.
577 Donnay, G. and Barton, R. Jr. (1972) Refinement of the crystal structure of elbaite and the
578 mechanism of tourmaline solid solution. Tschermaks Mineralogische und Petrographische
579 Mitteilungen, 18, 273–286.
580 Dyar, M.D., Taylor, M.E., Lutz, T.M., Francis, C.A., Guidotti, C.V., and Wise, M. (1998)
581 Inclusive chemical characterization of tourmaline: Mössbauer study of Fe valence and site
582 occupancy. American Mineralogist, 83, 848–864.
583 Dyar, M.D., Wiedenbeck, M., Robertson, D., Cross, LR., Delaney, J.S., Ferguson, K., Francis,
584 C.A., Grew, E.S., Guidotti, C.V., Hervig, R.L., Hughes, J.M., Husler, J., Leeman, W.,
585 McGuire, A.V., Rhede, D., Rothe, H., Paul, R.L., Richards, I., and Yates, M. (2001) Reference
586 minerals for the microanalysis of light elements. Geostandards Newsletter, 25, 441–463.
587 Ertl, A. (1995) Elbait, Olenit, Dravit-Buergerit-Mischkristalle, Dravit, Uvit und ein neuer Al-
588 Turmalin (?) von österreichischen Fundstellen. Mitteilungen der Österreichischen
589 Mineralogischen Gesellschaft, 140, 55–72.
590 Ertl, A. and Tillmanns, E. (2012) The [9]-coordinated *X* site in the crystal structure of tourmaline-
591 group minerals. Zeitschrift für Kristallographie, 227, 456–459.

592 Ertl, A. and Bačík, P. (2020) Considerations about Bi and Pb in the crystal structure of Cu-
593 bearing tourmaline. Minerals, 10, 706.
594 Ertl, A., Pertlik, F., and Bernhardt, H.-J. (1997) Investigations on olenite with excess boron from
595 the Koralpe, Styria, Austria. Österreichische Akademie der Wissenschaften, Mathematisch-
596 Naturwissenschaftliche Klasse, Abt. I, Anzeiger, 134, 3–10.
597 Ertl, A., Hughes, J.M., Pertlik, F., Foit F.F. Jr., Wright, S.E., Brandstätter, F., and Marler, B.
598 (2002) Polyhedron distortions in tourmaline. Canadian Mineralogist, 40, 153–162.
599 Ertl, A., Hughes, J.M., Brandstätter, F., Dyar, M.D., and Prasad, P.S.R. (2003) Disordered Mg-
600 bearing olenite from a granitic pegmatite at Goslarn, Austria: a chemical, structural and
601 infrared spectroscopic study. Canadian Mineralogist, 41, 1363–1370.
602 Ertl, A., Schuster, R., Prowatke, S., Brandstätter, F., Ludwig, T., Bernhardt, H.-J., Koller, F., and
603 Hughes, J.M. (2004) Mn-rich tourmaline and fluorapatite in a Variscan pegmatite from
604 Eibenstein an der Thaya, Bohemian massif, Lower Austria. European Journal of Mineralogy,
605 16, 551–560.
606 Ertl, A., Rossmann, G.R., Hughes, J.M., Prowatke, S., and Ludwig, T. (2005) Mn-bearing "oxy-
607 rossmanite" with tetrahedrally coordinated Al and B from Austria: Structure, chemistry, and
608 infrared and optical spectroscopic study. American Mineralogist, 90, 481–487.
609 Ertl, A., Hughes, J.M., Prowatke, S., Ludwig, T., Brandstätter, F., Körner, W., and Dyar, M.D.
610 (2007) Tetrahedrally-coordinated boron in Li-bearing olenite from "mushroom" tourmaline
611 from Momeik, Myanmar. Canadian Mineralogist, 45, 891–899.
612 Ertl, A., Tillmanns, E., Ntaflos, T., Francis, C., Giester, G., Körner, W., Hughes, J.M., Lengauer,
613 C., and Prem, M. (2008) Tetrahedrally coordinated boron in Al-rich tourmaline and its
614 relationship to the pressure-temperature conditions of formation. European Journal of
615 Mineralogy, 20, 881–888.

Ertl, A., Kolitsch, U., Meyer, H.-P., Ludwig, T., Lengauer, C.L., Nasdala, L., and Tillmanns, E. (2009) Substitution mechanism in tourmalines of the fluor-elbaite–rossmanite series from Wolkenburg, Saxony, Germany. Neues Jahrbuch Mineralogie, Abhandlungen, 186, 51–61.

Ertl, A., Rossman, G.R., Hughes, J.M., London, D., Wang, Y., O'Leary, J.A., Dyar, M.D., Prowatke, S., Ludwig, T., and Tillmanns, E. (2010) Tourmaline of the elbaite-schorl series from the Himalaya Mine, Mesa Grande, California, USA: A detailed investigation. American Mineralogist, 95, 24–40.

Ertl, A., Giester, G., Ludwig, T., Meyer, H.-P., and Rossman, G.R. (2012a) Synthetic B-rich olenite: Correlations of single-crystal structural data. American Mineralogist, 97, 1591–1597.

Ertl, A., Kolitsch, U., Dyar, M.D., Hughes, J.M., Rossman, G.R., Pieczka, A., Henry, D.J., Pezzotta, F., Prowatke, S., Lengauer, C.L., Körner, W., Brandstätter, F., Francis, C.A., Prem, M., and Tillmanns, E. (2012b) Limitations of Fe^{2+} and Mn^{2+} site occupancy in tourmaline: evidence from Fe^{2+}- and Mn^{2+}-rich tourmaline. American Mineralogist, 97, 1402–1416.

Ertl, A., Giester, G., Schüssler, U., Brätz, H., Okrusch, M., Tillmanns, E., and Bank, H. (2013) Cu- and Mn-bearing tourmalines from Brazil and Mozambique: Crystal structures, chemistry and correlations. Mineralogy and Petrology, 107, 265–279.

Ertl, A., Vereshchagin, O.S., Giester, G., Tillmanns, E., Meyer, H.-P., Ludwig, T., Rozhdestvenskaya, I.V., and Frank-Kamenetskaya, O.V. (2015) Structural and chemical investigation of a zoned synthetic Cu-rich tourmaline. Canadian Mineralogist, 53, 209–220.

Ertl, A., Henry, D.J., and Tillmanns, E. (2018) Tetrahedral substitutions in tourmaline: A review. European Journal of Mineralogy, 30, 465–470.

Ertl, A., Hughes, J.M., Prowatke, S., Ludwig, T., Lengauer, C.L., and Meyer, H.-P. (2020) Alumino-oxy-rossmanite, IMA 2020-008b, in: CNMNC Newsletter 58, European Journal of. Mineralogy, 32, 651.

640 Ferri, F., Poli, S., and Vielzeuf, D. (2009) An experimental determination of the effect of bulk
641 composition on phase relationships in metasediments at near-solidus conditions. Journal of
642 Petrology, 50, 909-931.
643 Foit, F.F., Jr. (1989) Crystal chemistry of alkali-deficient schorl and tourmaline structural
644 relationships. American Mineralogist, 74, 422–431.
645 Foit, F.F., Jr. and Rosenberg, P.E. (1979) The structure of vanadium-bearing tourmaline and its
646 implications regarding tourmaline solid solutions. American Mineralogist, 64, 788–798.
647 Götzinger, M.A., Beran, A., and Libowitzky, E. (1994) Exkursion A: Mineralvorkommen und
648 Lagerstätten im östlichen Waldviertel. Mitteilungen der Österreichischen Mineralogischen
649 Gesellschaft, 139, 389–405.
650 Grew, E.S., Chernosky, J.V., Werding, G., Abraham, K., Marquez, N., and Hinthorne, J.R.
651 (1990) Chemistry of kornerupine and associated minerals, a wet chemical, ion microprobe,
652 and X-ray study emphasizing Li-contents, Be-contents, B-contents and F-contents. Journal of
653 Petrology, 31, 1025–1070.
654 Grew, E.S., Yates, M.G., Shearer, C.K., and Wiedenbeck, M. (1997) Werdingite from the
655 Urungwe district, Zimbabwe. Mineralogical Magazine, 61, 713–718.
656 Hawthorne, F.C. (1996) Structural mechanisms for light-element variations in tourmaline.
657 Canadian Mineralogist, 34, 123–132.
658 Hawthorne, F.C. (2002) Bond-valence constraints on the chemical composition of tourmaline.
659 Canadian Mineralogist, 40, 789–797.
660 Hawthorne, F.C. (2016) Short-range atomic arrangements in minerals. I: The minerals of the
661 amphibole, tourmaline and pyroxene supergroups. European Journal of Mineralogy, 28, 513–
662 536.

663 Hawthorne, F.C. and Henry, D.J. (1999) Classification of the minerals of the tourmaline group.
664 European Journal of Mineralogy, 11, 201–215.
665 Hawthorne, F.C., MacDonald, D.J., and Burns, P.C. (1993) Reassignment of cation site-
666 occupancies in tourmaline: Al-Mg disorder in the crystal structure of dravite. American
667 Mineralogist,78, 265–270.
668 Henry, D.J. and Dutrow, B.L. (1996) Metamorphic tourmaline and its petrologic applications.
669 Reviews in Mineralogy and Geochemistry, 33, 503–557.
670 Henry, D.J., Novák, M., Hawthorne, F.C., Ertl, A., Dutrow, B.L., Uher, P., and Pezzotta, F.
671 (2011) Nomenclature of the tourmaline-supergroup minerals. American Mineralogist, 96,
672 895–913.
673 Hinton, R.W. (1990) Ion microprobe trace-element analysis of silicates: Measurement of multi-
674 element glasses. Chemical Geology, 83, 11–25.
675 Hinton, R.W. (1995) Ion microprobe analysis in geology. In: Potts, P.J, Bowles, J.F.W., Reed,
676 S.J.B. and Cave, R.M. (eds) Microprobe Techniques in the Earth Sciences, 235–289.
677 Huebner, J.S. (1969) Stability relations of rhodochrosite in the system manganese-carbon-
678 oxygen. American Mineralogist, 54, 457–481.
679 Hughes, J.M., Ertl, A., Dyar, M.D., Grew, E.S., Shearer, C.K., Yates, M.G., and Guidotti, C.V.
680 (2000) Tetrahedrally coordinated boron in a tourmaline: boron-rich olenite from Stoffhütte,
681 Koralpe, Austria. Canadian Mineralogist, 38, 861–868.
682 Hughes, J.M., Ertl, A., Dyar, M.D., Grew, E.S., Wiedenbeck, M., and Brandstätter, F. (2004)
683 Structural and chemical response to varying $^{[4]}$B content in zoned Fe-bearing olenite from
684 Koralpe, Austria. American Mineralogist, 89, 447–454.

685 Hughes, J.M., Rakovan, J., Ertl, A., Rossman, G.R., Baksheev, I., and Bernhardt, H.-J. (2011)
686 Dissymetrization in tourmaline: The atomic arrangement of sectorally zoned triclinic Ni-
687 bearing dravite. Canadian Mineralogist, 49, 29–40.
688 Kolitsch, U., Löffler, E., Schillhammer, H., Knobloch, G., and Lamatsch, P. (2020) 2178). Baryt,
689 Bertrandit, Columbit-(Mn), Eulytin, Hübnerit, rosa Olenit, Pezzottait(?), Pollucit, Rutil,
690 Scheelit, Stibarsen, „Uranmikrolith“ und gediegen Wismut sowie ein neues Cs-Al-Phosphat in
691 einem rosa Turmaline enthaltenden Pegmatit im Steinbruch von Eibenstein im Waldviertel,
692 Niederösterreich: ein Vorbericht. Pp. 191-200 in Walter, F., Auer, C., Bernhard, F., Bojar, H.-
693 P., Brandstätter, F., Grill, J. A., Kiseljak, R., Knobloch, G., Kolitsch, U., Lamatsch, P., Lenz,
694 C., Löffler, E., Melcher, F., Postl, W., Prasnik, H., Rausch, L., Reicht, M., Schachinger, T.,
695 Schillhammer, H., Schreieck, E., Schwabl, S., Steck, C., Steiner, T., Trattner, W., and
696 Weißensteiner, G. (2020) Neue Mineralfunde aus Österreich LXIX. Carinthia II, 210./130.,
697 153–218.
698 Ksanda, C.J. and Merwin, H.E. (1939) Improved technique in micropycnometric density
699 determination. American Mineralogist, 24, 482–484.
700 Lindner, M., Dörr, W., Reither, D., and Finger, F. (2020) The Dobra Gneiss and the Drosendorf
701 Unit in the southeastern Bohemian Massif, Austria: West Amazonian crust in the heart of
702 Europe. Geological Society, London, Special Publications, 503, 185–207.
703 Ludwig, T. and Stalder, R. (2007) A new method to eliminate the influence of in situ
704 contamination in SIMS analysis of hydrogen. Journal of Analytical Atomic Spectrometry,
705 22, 1415–1419.
706 Lussier, A.J., Aguiar, P.M., Michaelis, V.K., Kroeker, S., and Hawthorne, F.C. (2009) The
707 occurrence of tetrahedrally coordinated Al and B in tourmaline: An ^{11}B and ^{27}Al MAS NMR
708 study. American Mineralogist, 94, 785–792.

MacDonald, D.J. and Hawthorne, F.C. (1995) The crystal chemistry of Si ↔Al substitution in tourmaline. Canadian Mineralogist, 33, 849–858.

Mattson, S.M. (1985) Optical expressions of ion-pair interactions in minerals. Ph.D. Thesis, California Institute of Technology, Pasadena, U.S.A..

Ottolini, L., Bottazzi, P., and Vannucci, R. (1993) Quantification of lithium, beryllium, and boron in silicates by secondary ion mass spectrometry using conventional energy filtering. Analytical Chemistry, 65, 1960–1968.

Pearce N.J.G., Perkins W.T., Westgate J.A., Gorton M.P., Jackson S.E., Neal C.R., and Chenery S.P. (1997) A compilation of new and published major and trace element data for NIST SRM 610 and SRM 612 partially certified glass reference materials. Geostandards Newsletter: The Journal of Geostandards and Geoanalysis, 21, 115-144.

Petrakakis, K. (1997) Evolution of Moldanubian rocks in Austria: Review and synthesis. Journal of Metamorphic Geology, 15, 203–222.

Pouchou, J.-L. and Pichoir, F. (1991) Quantitative analysis of homogeneous or stratified microvolumes applying the model "PAP". In Electron Probe Quantitation; Heinrich, K.F.J., Newbury, D.E., eds., Plenum Press: New York, NY, USA, 1991; pp. 3l–75.

Povondra, P. and Čech, A. (1976) A method for the chemical analysis of tourmaline. Acta Universitatis Carolinae Geologica, 1976, 209–218.

Reinitz, I.L. and Rossman, G.R. (1988) Role of natural radiation in tourmaline coloration. American Mineralogist, 73, 822–825.

Selway, J.B., Novák, M., Hawthorne, F., Černý, P., Ottolini, L., and Kyser, T.K. (1998) Rossmanite, □$(LiAl_2)Al_6(Si_6O_{18})(BO_3)_3(OH)_4$, a new alkali-deficient tourmaline: Description and crystal structure. American Mineralogist, 83, 896–900.

Sheldrick, G.M. (2002) *SADABS Area-Detector Absorption Correction Program*. Bruker AXS Inc., Madison, Wisconsin.

Sheldrick, G.M. (2008) A short history of *SHELX*. Acta Crystallographica, A64, 112–122.

Sorger, D. (2020) Metamorphic and tectonic evolution of the Drosendorf and Gföhl units – Lower Austria, Bohemian Massif. Dissertation, Karl-Franzens-Universität Graz, Graz, Austria, 127 pp.

Syromyatnikov, F.V. (1935) The micropycnometric method for the determination of specific gravities of minerals. American Mineralogist, 20, 364–370.

Van Hinsberg, V.J. and Schumacher, J.C. (2007) Using estimated thermodynamic properties to model accessory phases: the case of tourmaline. Journal Metamorphic Geology, 25, 769–779.

Van Hinsberg, V.J., Henry, D.J., and Dutrow, B.L. (2011) Tourmaline as a petrologic forensic mineral: a unique recorder of its geologic past. Elements, 7, 327–332.

Tables

TABLE 1. Composition of pink tourmaline from the Hengl quarry, Eibenstein an der Thaya, Lower Austria.

	PINK1[1]	PINK2[2]
Constituent	wt%	wt%
SiO_2	33.96(28)	33.82(36)
TiO_2	0.10(3)	0.17(2)
Al_2O_3	47.08(16)	45.71(36)
B_2O_3	11.77(12)	12.12
FeO_{total}	0.29(8)	0.07(2)
FeO^*	0.08	0.02
$Fe_2O_3^*$	0.23	0.06
MnO_{total}	2.05(9)	2.33(19)
MnO^*	0.52	0.61
$Mn_2O_3^*$	1.70	1.92
CaO	0.04(2)	0.09(1)
Li_2O	0.25(1)	0.46
ZnO	0.03(1)	0.02(1)
Na_2O	1.51(5)	1.84(4)
H_2O	2.79**	2.90***
F	0.09(2)	0.43(10)
$O \equiv F$	-0.04	-0.18
Total	100.11	100.00

Notes: [1] Type material of alumino-oxy-rossmanite from 1994 pegmatite; average of 25 EMP analyses and average of two SIMS analyses for B_2O_3, Li_2O, BeO, and H_2O. BeO = 9 µg/g, H_2O = 2.98(9) wt%. [2] Tourmaline from 2017 pegmatite (details see text); average of 20 EMP analyses and one SIMS analysis for B_2O_3, Li_2O, and H_2O. *Valence states were estimated by applying the Beer's Law epsilon value to the optical absorption spectrum (details see text). **Weight percent

782 calculated from optimal site occupancies (details see Ertl et al. 2015). ***This value was
783 calculated to produce a total sum of 100%. The measured SIMS value of H_2O was 3.37 wt% (one
784 analysis). Hence, the calculated value is within an error of 14% in good agreement with the
785 measured value and with other observed data (further details see text).

786 **TABLE 2.** Selected structural data (Å) of Al-rich oxy-tourmaline from the Hengl quarry,

787 Eibenstein an der Thaya, Lower Austria.

788		PINK1[1]	PINK2[2]
789	*a*	15.803(1)	15.809(1)
790	*c*	7.088(1)	7.082(1)
791	<X–O>	2.687(2)	2.680(1)
792	<Y–O>	1.962(1)	1.970(1)
793	<Z–O>	1.908(1)	1.907(1)
794	<T–O>	1.619(1)	1.617(1)

795 *Notes:* [1] Type material of alumino-oxy-rossmanite; pink tourmaline (with a major alumino-oxy-

796 rossmanite component) from 1994 pegmatite. [2] Pink tourmaline from 2017 pegmatite (details see

797 text).

798

This is the peer-reviewed, final accepted version for American Mineralogist, published by the Mineralogical Society of America.
The published version is subject to change. Cite as Authors (Year) Title. American Mineralogist, in press.
DOI: https://doi.org/10.2138/am-2022-8047. http://www.minsocam.org/

799 **TABLE 3.** Chemical compositions and unit-cell parameters of alumino-oxy-rossmanite compared
800 with IMA-approved Al-rich and Li-bearing tourmalines.
801

	1	2	3	4	5	6
SiO_2	33.96	38.10	37.08	37.48	38.38	37.70
Al_2O_3	47.08	44.60	38.37	37.81	43.49	37.90
B_2O_3	11.77	10.88	10.81	10.83	11.01	10.89
Li_2O	0.25	1.13	1.59	1.58	1.63	2.48
Na_2O	1.51	1.43	2.58	2.51	1.92	0.88
CaO	0.04	-	0.42	0.34	0.05	4.21
H_2O	2.99	3.70	3.03	3.03	2.86	2.69
F	0.09	0.20	0.62	1.49	0.71	1.72
TiO_2	0.10	-	0.03	-	-	0.38
FeO	0.29	-	2.99	3.39	-	0.83
MnO	2.05	-	1.39	2.09	0.02	0.27
MgO	-	-	0.03	-	-	0.11
K_2O	-	-	0.31	0.06	-	-
a (Å)	15.803	15.770	15.882	15.893	15.823	15.867
c (Å)	7.088	7.085	7.122	7.122	7.095	7.135
V (Å^3)	1532.9	1525.9	1555.8	1558.0	1538.4	1555.7

802
803 *Notes:* 1: pink alumino-oxy-rossmanit from the Hengl quarry, Eibenstein, Lower Austria (PINK1,
804 this work); 2: pale pink rossmanite, type locality Rožná, Czech Republic (Selway et al. 1998); 3:
805 green elbaite, Dolní Bory, Czech Republic (Povondra et al. 1985); 4: green fluor-elbaite, type
806 locality Cruzeiro mine, Minas Gerais, Brazil (Bosi et al. 2013); 5: pale pink darrellhenryite, type
807 locality Nová Ves, Czech Republic (Novák et al. 2013); 6: fluor-liddicoatite, type locality near
808 Antsirabe, Madagascar (Dunn et al. 1977).
809

This is the peer-reviewed, final accepted version for American Mineralogist, published by the Mineralogical Society of America.
The published version is subject to change. Cite as Authors (Year) Title. American Mineralogist, in press.
DOI: https://doi.org/10.2138/am-2022-8047. http://www.minsocam.org/

Supplemental Tables

TABLE S1. Complete calculated X-ray powder diffraction data (Cu*K*α) for alumino-oxy-rossmanite.

h	*k*	*l*	$d_{calc.}$	$I_{calc.}$
1	1	0	7.9015	2
1	**0**	**1**	**6.2938**	**28**
0	2	1	4.9229	23
0	3	0	4.5620	17
2	**1**	**1**	**4.1783**	**61**
2	**2**	**0**	**3.9508**	**85**
0	**1**	**2**	**3.4307**	**55**
1	3	1	3.3461	15
4	0	1	3.0812	4
1	4	0	2.9865	17
1	**2**	**2**	**2.9236**	**78**
3	2	1	2.8707	8
3	3	0	2.6338	2
3	1	2	2.5904	7
0	**5**	**1**	**2.5534**	**100**
2	4	1	2.4297	4
0	0	3	2.3626	10
2	3	2	2.3501	13
5	1	1	2.3224	22
0	6	0	2.2810	2
5	0	2	2.1663	9
4	3	1	2.1445	13
0	3	3	2.0979	6
3	0	3	2.0979	5
4	2	2	2.0892	7
2	2	3	2.0277	12
1	**5**	**2**	**2.0198**	**39**
1	6	1	2.0021	8
4	4	0	1.9754	2
3	**4**	**2**	**1.8995**	**30**
3	5	1	1.8847	2
1	4	3	1.8529	5
6	2	1	1.8333	8
3	3	3	1.7587	6
1	0	4	1.7573	3
0	2	4	1.7154	2
2	6	2	1.6731	4

0 6 3	1.6410	16
6 0 3	1.6410	3
2 7 1	1.6273	12
5 5 0	1.5803	14
4 0 4	1.5734	3
4 5 2	1.5708	4
8 1 1	1.5624	3
3 2 4	1.5431	2

Notes: Calculated using single-crystal structural data of sample PINK1. Only reflections with I_{calc} > 1 are listed. The eight strongest reflections are in bold.

This is the peer-reviewed, final accepted version for American Mineralogist, published by the Mineralogical Society of America.
The published version is subject to change. Cite as Authors (Year) Title. American Mineralogist, in press.
DOI: https://doi.org/10.2138/am-2022-8047. http://www.minsocam.org/

865 **TABLE S2.** Theoretical compositions of known and potential Al-rich and Li-bearing tourmalines.
866

	1	2	3	4	5	6	7	8
SiO_2	31.90	38.65	39.03	38.49	38.40	38.12	37.41	38.12
Al_2O_3	54.14	46.45	44.15	40.82	40.73	43.12	47.61	37.73
B_2O_3	11.09	11.20	11.30	11.15	11.12	11.04	10.84	11.04
Li_2O	-	0.80	1.62	2.39	2.39	1.58	-	3.16
Na_2O	-	-	-	3.31	3.30	3.28	3.22	-
CaO	-	-	-	-	-	-	-	5.93
H_2O	2.87	2.90	3.90	3.85	2.88	2.86	0.93	2.86
F	-	-	-	-	2.02	-	-	2.01
X site	□	□	□	Na	Na	Na	Na	Ca
Y site	Al_3	$Al_{2.5}Li_{0.5}$	Al_2Li	$Li_{1.5}Al_{1.5}$	$Li_{1.5}Al_{1.5}$	Al_2Li	Al_3	Li_2Al
Z site	Al_6	Al_6	Al_6	Al_6	Al_6	Al_6	Al_6	Al_6
B site	B_3	B_3	B_3	B_3	B_3	B_3	B_3	B_3
T site	Si_5Al	Si_6	Si_6	Si_6	Si_6	Si_6	Si_6	Si_6
V site	$(OH)_3$	$(OH)_3$	$(OH)_3$	$(OH)_3$	$(OH)_3$	$(OH)_3$	$O_2(OH)^*$	$(OH)_3$
W site	O	O	OH	OH	F	O	O^*	F

867
868 *Notes:* 1: Alumino-oxy-rossmanite, $\square Al_3Al_6(Si_5AlO_{18})(BO_3)_3(OH)_3O$; 2 "oxy-rossmanite",
869 $\square(Li_{0.5}Al_{2.5})Al_6Si_6O_{18}(BO_3)_3(OH)_3O$; 3: Rossmanite, $\square(LiAl_2)Al_6Si_6O_{18}(BO_3)_3(OH)_3OH$; 4:
870 Elbaite, $Na(Li_{1.5}Al_{1.5})Al_6Si_6O_{18}(BO_3)_3(OH)_3OH$; 5: Fluor-elbaite,
871 $Na(Li_{1.5}Al_{1.5})Al_6Si_6O_{18}(BO_3)_3(OH)_3F$; 6: Darrellhenryite, $Na(LiAl_2)Al_6Si_6O_{18}(BO_3)_3(OH)_3O$; 7:
872 Olenite $NaAl_3Al_6Si_6O_{18}(BO_3)_3(O)_3OH$; 8: Fluor-liddicoatite, $Ca(Li_2Al)Al_6Si_6O_{18}(BO_3)_3(OH)_3F$;
873 *To produce an ordered end-member formula of olenite, the (OH) group can be assigned to the V
874 site although it occupies the W site.
875

876 **Figure captions:**

877 **FIGURE 1.** Pink core of alumino-oxy-rossmanite (type material, PINK1) with a dark green rim of
878 Fe-bearing alumino-oxy-rossmanite in quartz. Found in 1994 in the Hengl quarry, near the village
879 Eibenstein an der Thaya, Lower Austria (photo detail ~7 × 13 mm^2). Collection A.P.

880

881 **FIGURE 2.** Pink tourmaline with a major alumino-oxy-rossmanite component (PINK2) in quartz.
882 Found in 2017 in the Hengl quarry, near the village Eibenstein an der Thaya, Lower Austria
883 (photo detail ~15 × 22 mm^2). Collection A.P.

884

885 **FIGURE 3.** Optical absorption spectrum of a 0.0928 mm thick crystal of alumino-oxy-rossmanite
886 (sample PINK1).

887

888 **FIGURE 4.** Near-infrared spectrum of alumino-oxy-rossmanite (sample PINK1) from Eibenstein
889 in the OH overtone region. A spectrum of a 0.0928 mm thick crystal was plotted normalized to
890 1.0 mm thickness.

891

892 **FIGURE 5.** Relationship between bond-angle distortion σ_{oct}^2 of the ZO_6 octahedron and the
893 average Y-O distance. Modified from Figure 3 from Ertl et al. (2002), including the structural
894 data from Hughes et al. (2004). Alumino-oxy-rossmanite (type material, PINK1), Al-rich oxy-
895 tourmaline (with a major alumino-oxy-rossmanite component, PINK2).

896

897 **FIGURE 6.** Total Al versus Si in different Al-rich tourmaline end-members. Note: a: Olenite; b:
898 Darrellhenryite; c: Elbaite, fluor-elbaite; d: Fluor-liddicoatite. Measured samples: PINK1:

899 Alumino-oxy-rossmanite (type material); PINK2: Pink tourmaline with a major alumino-oxy-
900 rossmanite component.
901
902 **FIGURE 7.** Total Al versus Li in Al-rich tourmaline end-members. Note: a: Olenite; b:
903 Darrellhenryite; c: Elbaite, fluor-elbaite; d: Fluor-liddicoatite. Measured samples: PINK1:
904 Alumino-oxy-rossmanite (type material); PINK2: Pink tourmaline with a major alumino-oxy-
905 rossmanite component.
906
907

Fig 1

Fig 2

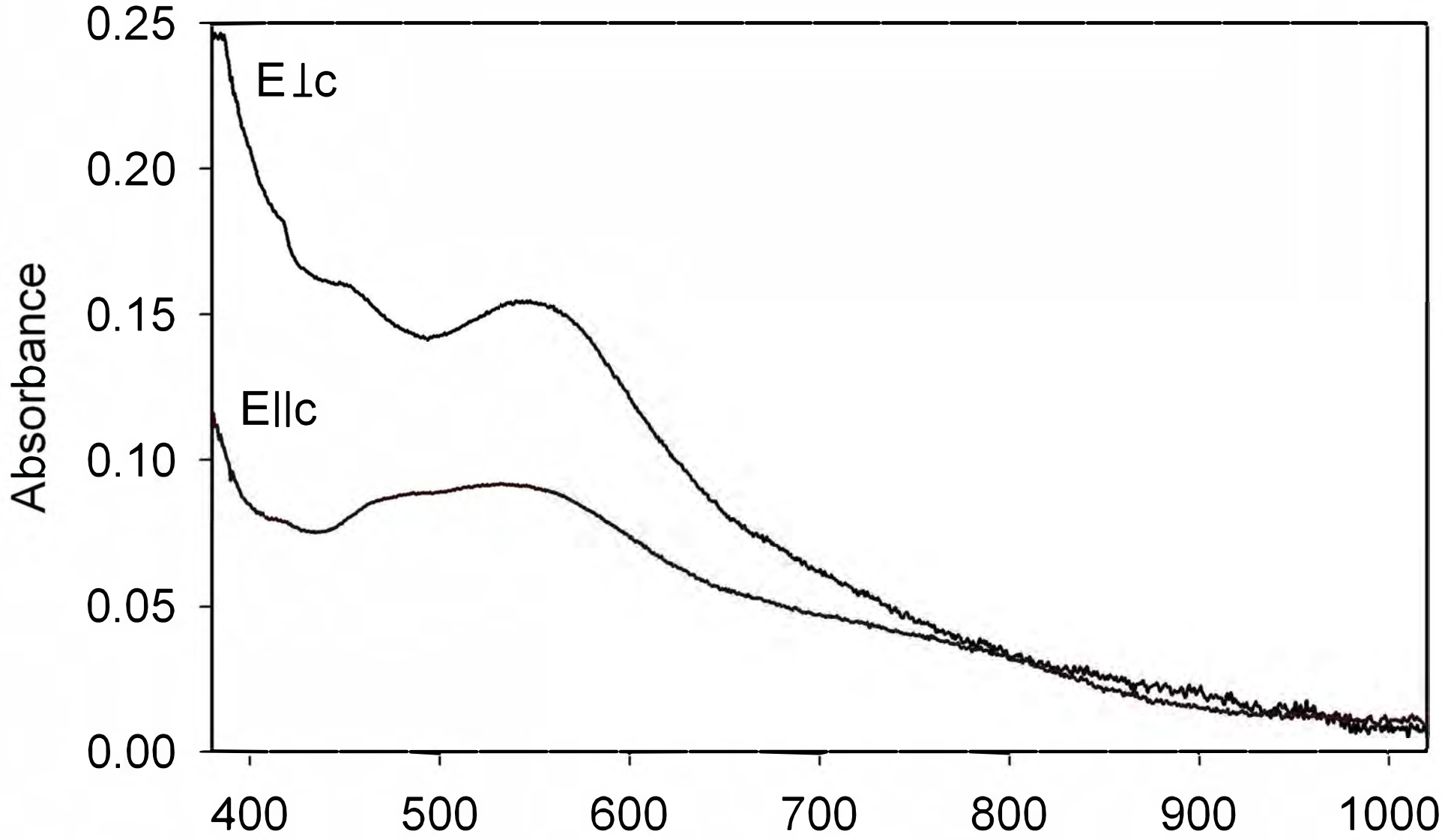
0.25
0.20
0.15
0.10
0.05
0.00
Absorbance
E⊥c
E||c
400
500
600
700
800
900
1000
Wavelength, nm

Fig 3

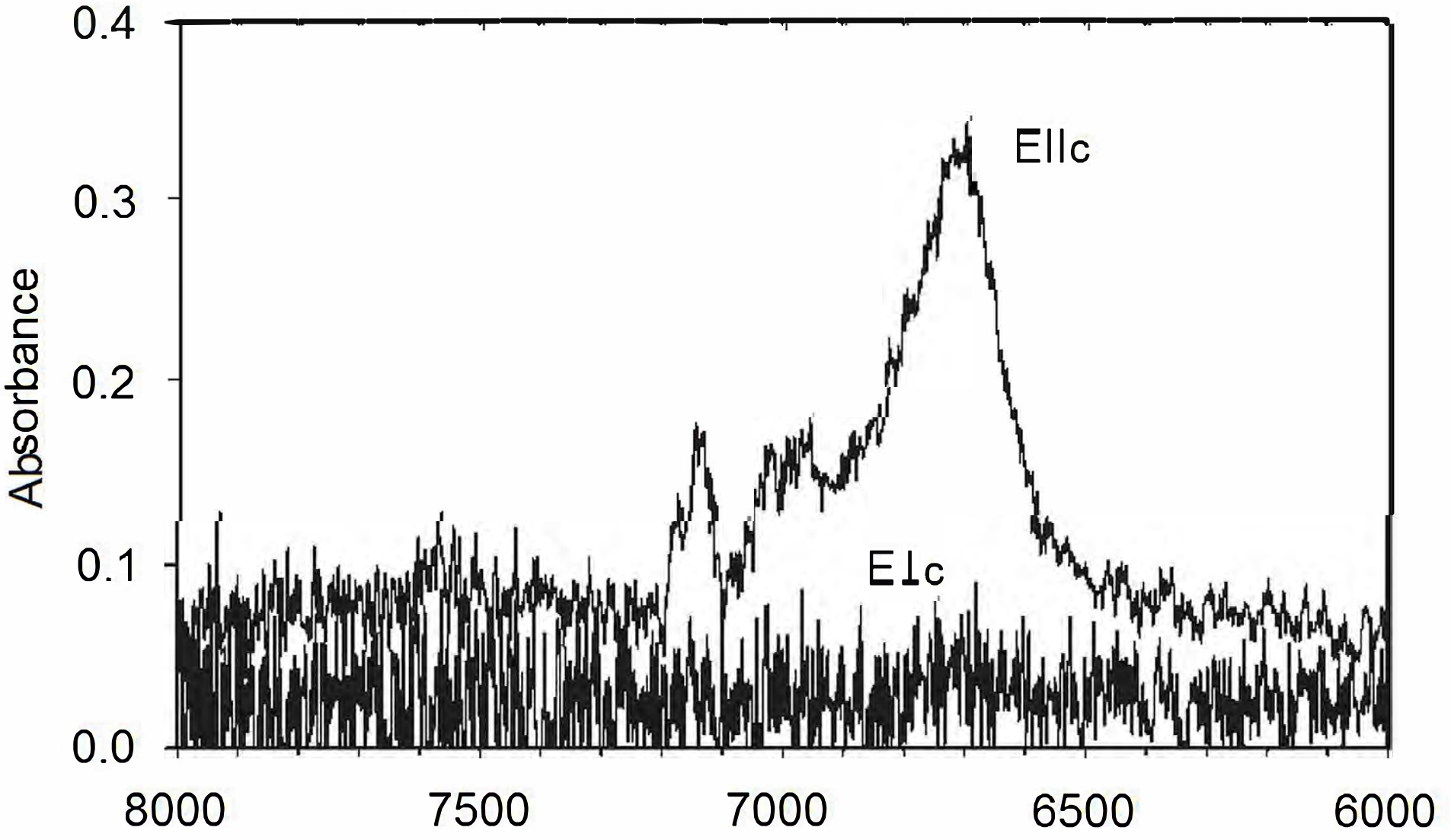
0.4
0.3
0.2
0.1
0.0
Absorbance
E||c
E⊥c
8000
7500
7000
6500
6000
Wavenumber, cm-1

Fig 4

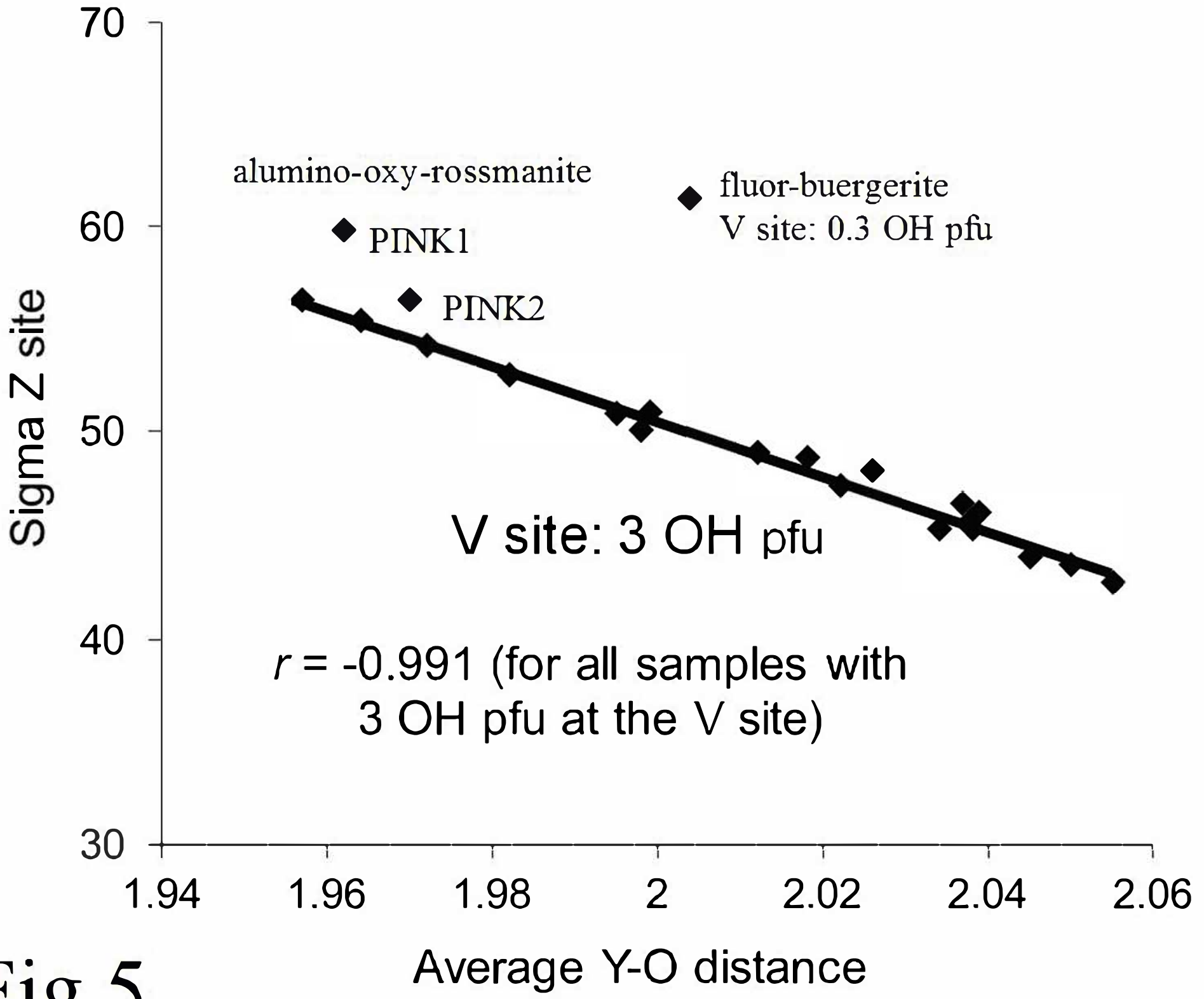
70
60
50
40
30
Sigma Z site
alumino-oxy-rossmanite
PINK1
PINK2
fluor-buergerite
V site: 0.3 OH pfu
V site: 3 OH pfu
r = -0.991 (for all samples with
3 OH pfu at the V site)
1.94
1.96
1.98
2
2.02
2.04
2.06
Average Y-O distance

Fig 5

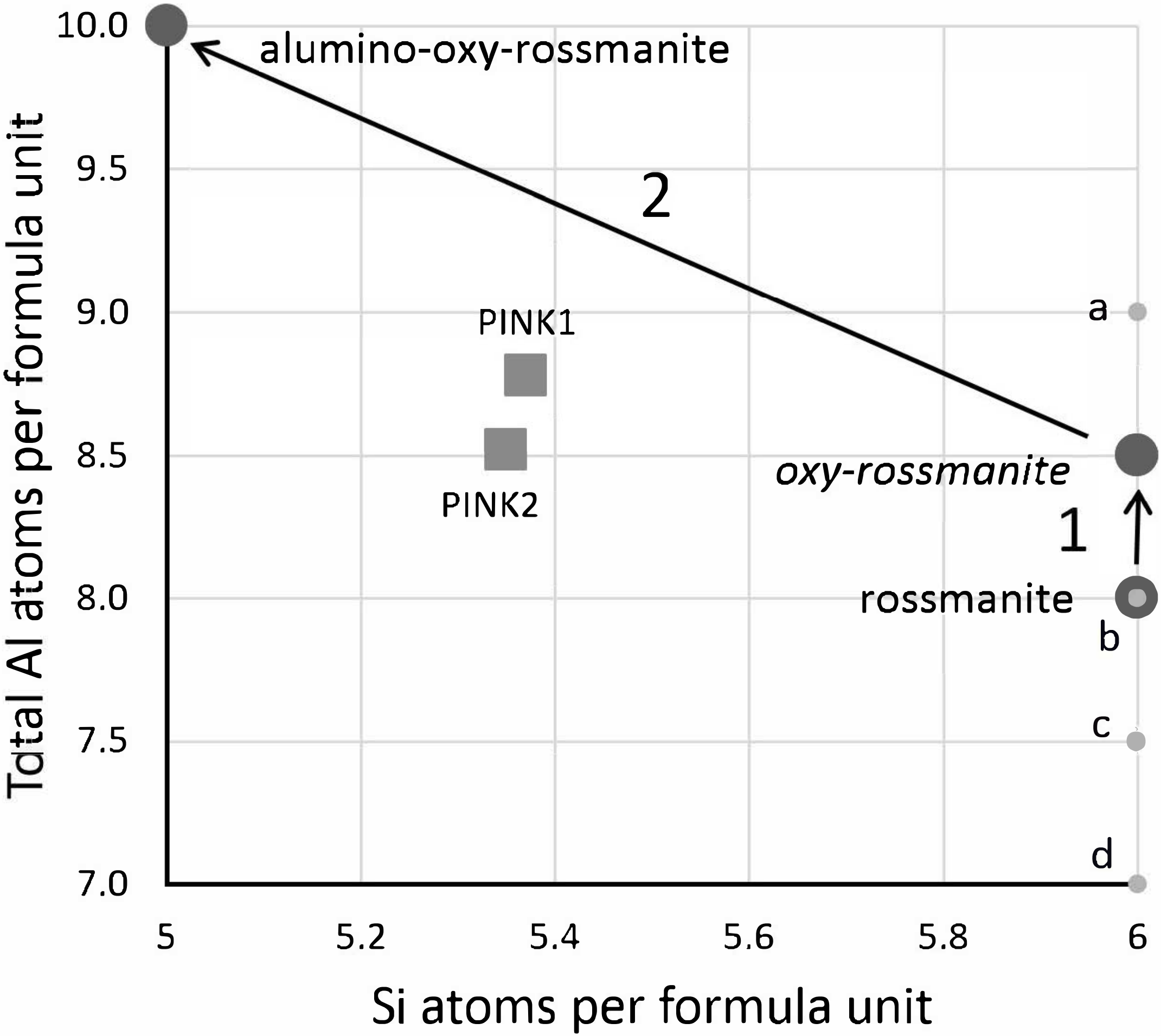
alumino-oxy-rossmanite
2
PINK1
PINK2
a
oxy-rossmanite
1
rossmanite
b
c
d
10.0
9.5
9.0
8.5
8.0
7.5
7.0
Total Al atoms per formula unit
5
5.2
5.4
5.6
5.8
6
Si atoms per formula unit

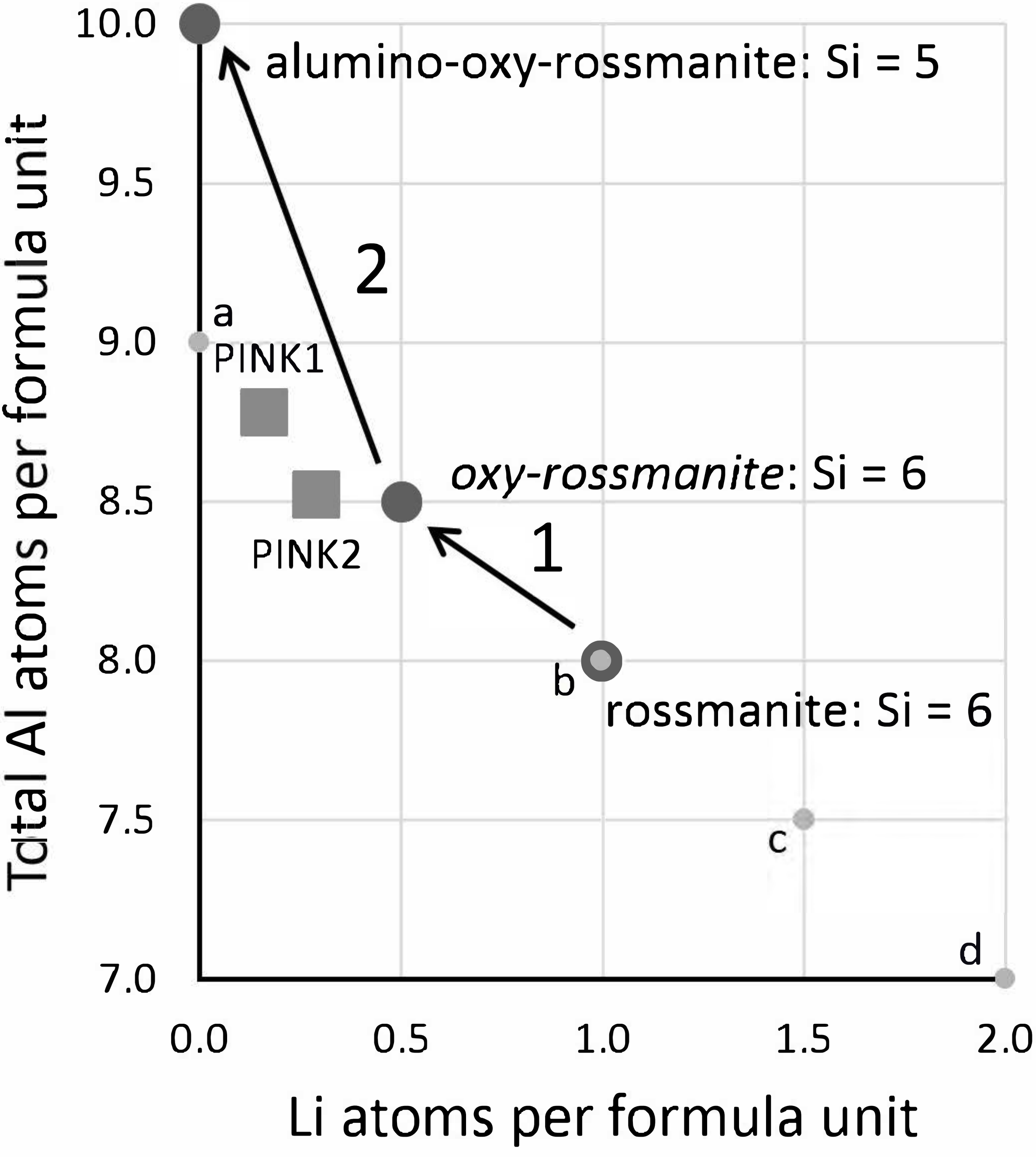
alumino-oxy-rossmanite: Si = 5
2
a
PINK1
PINK2
oxy-rossmanite: Si = 6
1
b
rossmanite: Si = 6
c
d
10.0
9.5
9.0
8.5
8.0
7.5
7.0
Total Al atoms per formula unit
0.0
0.5
1.0
1.5
2.0
Li atoms per formula unit